Carbohydrate Polymers 375 (2026) 124803

Contents lists available at ScienceDirect

Carbohydrate Polymers

journal homepage: www.elsevier.com/locate/carbpol

Engineered cytosolic and chloroplastic UDP-glucose epimerases distinctly modulate xylan interplay for size-tunable cellulose nanocrystals production in *Oryza sativa*

Yumeng Sun [a,1], Muzi Li [a,1], Meiyun Yang [b], Wennian Xia [b], Sha Wang [b], Zhongyi Wang [b], Yanting Wang [c], Liangcai Peng [c], Huizhen Hu [b,*], Ran Zhang [a,*]

[a] *Plant Cell Wall Biology Laboratory, School of Agriculture, Yunnan University, Kunming, 650091, China*
[b] *Plant Cell Wall Biology Laboratory, College of Landscape Architecture and Horticulture Sciences, Southwest Forestry University, Kunming, 650224, China*
[c] *Key Laboratory of Fermentation Engineering (Ministry of Education), National "111" Center for Cellular Regulation & Molecular Pharmaceutics, Hubei Key Laboratory of Industrial Microbiology, School of Life and Health Sciences, Hubei University of Technology, Wuhan, 430068, China*

ARTICLE INFO

Keywords:
UGE
Plant cell wall
Cellulose
Xylan
Plant mechanics
Rice

ABSTRACT

The plant cell wall is a complex matrix critical for structural integrity, growth, and biomass utilization. This study investigates the distinct roles of cytosolic and chloroplastic UDP-glucose epimerases (CytoUGE and CpUGE) in regulating cell wall assembly and mechanical strength in *Oryza sativa*. By genetic modulation, we demonstrate that both CytoUGE and CpUGE enhance photosynthesis and increase the content of cellulose, hemicellulose, and lignin, thereby improving stem mechanical strength. Notably, CpUGE exerts a more pronounced effect on cellulose crystallinity while reducing xylan interference with cellulose microfibrils. Detailed monosaccharide analysis reveals that CpUGE promotes tighter xylan-lignin interactions and lower arabinose substitution in alkali-insoluble xylan, contributing to a more ordered cell wall architecture. Atomic force microscopy reveals that cellulose nanocrystals (CNCs) derived from CytoUGE exhibit a tendency to self-aggregate, forming structures of significantly larger dimensions. Moreover, modulation of both UGEs bidirectionally tunes CNC dimensions—overexpression enhances mechanical reinforcement, while loss-of-function reduces CNC size to increase reactivity. Integrate analyses identify the alkali-insoluble and soluble arabinose/xylose ratios as key indicators linking cell wall structure to mechanics. Our findings reveal that spatially separated UGE differentially regulate xylan interplay, providing a strategic target for engineering rice with improved cellulose quality for both agricultural and industrial applications.

1. Introduction

The plant cell wall is a critical, complex matrix that regulates morphogenesis, biomechanical stability, and pathogen defense (Coen & Cosgrove, 2023; Cosgrove, 2022; Ishida & Noutoshi, 2022; Molina et al., 2024; Wan et al., 2021). Beyond its structural role, it also serves as the main carbon sink for photosynthetic products and represents Earth's most abundant source of renewable biopolymers (Li et al., 2024; Ray et al., 2021; Zhang, Gao, Wang, et al., 2023). Composed of cellulose, non-cellulosic polysaccharides, and lignin, the cell wall has its own distinct assembly for biological functions (Wang et al., 2016; Zhang, Gao, et al., 2021). Crucially, hemicelluloses act as dynamic interfacial linkers between cellulose and lignin microdomains (Cosgrove, 2018; Herburger et al., 2020; Wang et al., 2022). Given the heterogeneity and crosslinking of the matrix, concerted enhancement of both the biosynthesis and assembly of wall polymers is important. However, the certain metabolic pathways and regulatory mechanisms underlying the biosynthesis and assembly of lignocellulosic polymers for biological and biomaterial properties remain rarely reported.

Nucleotide sugars, as the active form of sugars, are the building blocks for the construction of plant cell wall polysaccharides, a process catalyzed by glycosyltransferases (Bar-Peled & O'Neill, 2011; Verbančič et al., 2018). Plants possess a diverse array of nucleotide sugars, whose production depends on an elaborate interconversion network.

* Correspondence authors.
E-mail addresses: Jenny_0129@swfu.edu.cn (H. Hu), zhangran@ynu.edu.cn (R. Zhang).
[1] These authors contributed equally to this work.

https://doi.org/10.1016/j.carbpol.2025.124803
Received 15 October 2025; Received in revised form 5 December 2025; Accepted 8 December 2025
Available online 9 December 2025

Accumulating evidence demonstrates that this intricate system integrates developmental, metabolic, and environmental cues to modulate glycosylation patterns, establishing these enzymes as pivotal regulators linking primary metabolism and extracellular matrix dynamics (Seifert, 2004; Seifert et al., 2004). Notwithstanding their critical role, the systematic engineering of nucleotide sugar interconversion pathways to optimize biomass composition and cross-linking remains largely unexplored.

UDP-glucose epimerase (UGE; EC 5.1.3.2) catalyzes bidirectional UDP-Glc/UDP-Gal conversion, functioning as a metabolic nexus (Barber et al., 2006). In *Arabidopsis*, five *UGE* genes are identified, with UGE2 and UGE4 being essential for growth through UDP-Gal provision (Rösti et al., 2007). Rice possesses four cytoplasmic UGE genes (OsUGE1–4), among which OsUGE2 (e.g., brittle culm mutant *Osfc24/uge2*) is functionally characterized. A nonsense mutation in this CytoUGE reduces cytoplasmic UDP-Gal supply, impairing galactolipid synthesis, chloroplast development, photosynthesis and cell wall formation (Liu et al., 2020; Zhang et al., 2020; Zhang, Wang, et al., 2021). Notably, an unannotated chloroplast-localized CpUGE protein exhibits UGE activity and is essential for galactolipid biosynthesis, thylakoid membrane formation, and biomass accumulation (Li et al., 2011). These findings establish distinct subcellular compartments for major UGE activities: CytoUGE dominates cytoplasmic metabolism while CpUGE operates in chloroplasts. This spatial separation creates dual UDP-Gal supply pathways in rice, suggesting potential for genetically improving plant growth and cell walls through isoform-specific engineering. However, how these compartmentalized UGE channels differentially regulate UDP-galactose metabolism for specialized cell wall assembly remains unresolved.

As a globally vital food crop, rice generates substantial lignocellulosic residues with significant biomaterial potential (Yu et al., 2025). Given the distinct rice subcellular localization of CytoUGE in the cytosol and CpUGE in the chloroplast, and their respective roles in galactolipid and cell wall biosynthesis, we hypothesize that these two rice UGE isoforms differentially regulate photosynthesis to modulate cell wall polymers assembly through spatially separated metabolic pathways. Specifically, we propose that CpUGE, by enhancing chloroplastic pathway and close to photosynthesis, exerts a more pronounced influence on cellulose accumulation, properties and its bioproduction. To test this hypothesis, we generated rice lines overexpressing CytoUGE or CpUGE and conducted integrated analyses of cell wall composition, polymer interplay, mechanical strength, and cellulose nanocrystal properties. This work aims to elucidate how compartmentalized nucleotide sugar metabolism can be leveraged to engineer rice with improved biomass quality for both agricultural resilience and industrial valorization.

2. Materials and methods

2.1. Genetic rice plants

The two genes, *CytoUGE* and *CpUGE*, were utilized to construct genetically engineered rice capable of modulating UDP-Galactose supply through cytosolic and chloroplastic pathways, respectively. To achieve overproduction of UDP-Galactose, the full-length cDNA sequences of these two genes were cloned from the *Nipponbare* cultivar and inserted into the plant binary vector pCAMBIA1300 (*pCAMBIA1300-Ubi::CytoUGE*) and pU1301 (*pU1301-Ubi::CpUGE-3FLAG*) under the control of the Ubi promoter, respectively. These constructs were then introduced into *Agrobacterium tumefaciens* strain EHA105 and subsequently transferred into the rice cultivar *Nipponbare* via *Agrobacterium*-mediated transformation. To generate rice plants with a deficiency in UDP-Galactose supply, the mutant *cyto-uge* was previously reported (Zhang et al., 2020), while *cp-uge* was created using the CRISPR-Cas9 gene-editing system. The single-guide RNA (sgRNA) targeting *CpUGE* was designed using the CRISPR-PLANT program. The corresponding oligonucleotides were cloned into the pRGEB32 vector (*pRGEB32-Ubi::cp-uge*) and transformed into wild-type rice calli using *Agrobacterium tumefaciens* strain EHA105 (Xie et al., 2015). CRISPR-Cas9 genome editing is validated by extracting DNA from edited samples and analyzing target loci: PCR-based assays detect insertions/deletions (indels), while Sanger/next-generation sequencing (NGS) resolves precise mutation profiles, enabling rigorous assessment of on-target editing efficiency and fidelity. Lines (*cp-uge*) harboring frameshift or nonsense mutations are then selected for downstream functional analysis to characterize the phenotypic consequences of targeted gene disruption. All primers used for gene cloning and screening are listed in Table S1.

2.2. Quantitative PCR

Total RNA was isolated from plant tissues using Trizol reagent (Invitrogen, Carlsbad, CA, USA) and subsequently reverse-transcribed into cDNA using an oligo-dT18 primer, DNase I, and M-MLV Reverse Transcriptase (Promega Kit). Quantitative PCR (qPCR) reactions were performed on a Bio-Rad MyCycler thermal cycler with the 2× SYBR Green qPCR Mix (ZF101, ZOMANBIO), following the manufacturer's instructions. The rice polyubiquitin gene (*OsUBQ1*) was employed as an internal control for normalization. Each sample was analyzed using at least two biological replicates, and each test was conducted in triplicate to ensure reliability. The relative quantification of transcript levels was calculated using the comparative Ct method. The expression value of *OsUBQ* was defined as 100, and the expression level of the *UGE* genes were thus normalized to the expression level of *OsUBQ*. Primers used in these assays are listed in Table S1. Three biological replications were performed.

2.3. Plant agronomic traits

At the rice heading stage, the 2nd internodes were chosen to test the mechanical properties under room temperature conditions. 9 biological independent internodes were selected for the test. The breaking force of the internodes was determined using a Prostrate Tester (DIK 7401, Daiki Rika Kogyo Co. Ltd., Japan) with the same fulcrum each time. At the rice mature stage, plant height and tiller number were assessed by selecting 9 biologically independent plants from each line.

2.4. Photosynthetic rate

Between ten and eleven o'clock on a cloudless morning, measurements of the photosynthetic rate, stomatal conductance, and transpiration rate were conducted on the uppermost fully expanded leaves using a LI-6800 portable photosynthesis system (LI-COR), following the procedures previously (Wang et al., 2018).

2.5. Cell wall polymer extraction and determination

The plant cell wall fractionation procedure was performed based on a previously reported method with minor modifications (Yu et al., 2022). Biomass samples of mature stem from WT (wild-type *Nipponbare*, NPB), CytoUGE, and CpUGE overexpression lines were subjected to sequential extraction steps to remove soluble sugars, lipids, starch, and pectin. Specifically, potassium phosphate buffer (pH 7.0), chloroform-methanol (1:1, v/v), DMSO-water (9:1, v/v), and ammonium oxalate 0.5 % (w/v) were successively employed for these extractions. Following this, the residual biomass was treated with 4 M KOH containing 1.0 mg/mL sodium borohydride at room temperature for 1 h. The resulting supernatants were pooled to obtain the KOH-extractable hemicellulose fraction. The non-KOH-extractable hemicellulose fraction was determined by analyzing the total pentose content in the remaining pellets. The total hemicellulose content was calculated as the sum of the pentose content in the non-KOH-extractable pellets and the total hexose and pentose contents in the KOH-extractable fraction. Crystalline cellulose levels

were quantified using the Updegraff method (Updegraff, 1969). Hexose and pentose contents were measured using colorimetric assays described previously (Xu et al., 2012). Finally, the total lignin content was determined using a two-step acid hydrolysis method following the Laboratory Analytical Procedure developed by the National Renewable Energy Laboratory.

2.6. Monosaccharide composition

Following dilution, the KOH-extractable hemicellulose fraction is neutralized with sulfuric acid to obtain a neutral solution. The non-KOH-extractable residues undergo complete hydrolysis with 67 % concentrated sulfuric acid and then neutralized with NaOH after dilution to obtain a neutral solution. The neutral solutions were subjected to hydrolysis using 2 M trifluoroacetic acid (TFA). The determination of neutral sugars was carried out using GC–MS (SHIMADZU GCMS-QP2010 Plus), following the previously described method with Myo-inositol internal standard (Xu et al., 2012). Three biological replicates were conducted to ensure reliability and repeatability.

2.7. Cellulosic CrI and molecular weight

The lignocellulosic samples of mature stem from WT, CytoUGE, and CpUGE overexpression lines were subjected to X-Ray diffraction (XRD) analysis using a Rigaku-D/MAX Ultima III instrument from Japan, following established protocols (Zhang, Hu, Peng, et al., 2023). The powders were placed on a glass holder and subjected to XRD measurements under controlled conditions. Ni-filtered Cu-Kα radiation with a wavelength of 0.154056 nm, generated at a voltage of 40 kV and current of 18 mA, was employed. Scans were conducted at a speed of 0.0197° s^{-1}, covering a range of 10° to 45°. The Crystallinity Index (CrI) was calculated using the equation:

$$\mathrm{CrI}\ (\%) = \frac{I_{200} - I_{am}}{I_{200}} \times 100$$

Here, I_{200} represents the intensity of the 2-Theta around 22.5°, which encompasses both crystalline and amorphous cellulose. I_{am} corresponds to the minimum intensity of the amorphous cellulose at 2-Theta around 18°.

The cellulose degree of polymerization was measured by the viscosity method (Zhang, Hu, Peng, et al., 2023), as described previously. The approximate molecular weight (M) of the cellulose is obtained by multiplying the degree of polymerization by the molecular weight of one glucose unit:

$$M = DP \times 162$$

2.8. Cell wall digestibility

To evaluate cell wall recalcitrance by testing its enzymatic digestibility, the same chemical pretreatments and mixed-cellulase hydrolysis were performed as previously described (Zhang et al., 2020). Initially, the cell wall samples of mature stem from WT, *CytoUGE*, and *CpUGE* overexpression lines were pretreated with 0.5 % NaOH at 50 °C for 2 h. Subsequently, the pretreated pellets were washed with distilled water until a neutral pH was achieved. The resulting pellets were then subjected to sequential enzymatic hydrolysis at 150 rpm and 50 °C for 48 h. The mixed-cellulases from Imperial Jade Biotechnology Co., Ltd. (Ningxia, China) were loaded at a dosage of 10.60 FPU/g biomass, while xylanase was loaded at 6.72 U/g biomass. After the enzymatic reactions, the supernatants were collected by centrifugation at 3000 *g* for 5 min to estimate the yield of total sugars (hexose and pentose). All experiments were conducted in triplicate. The hexose yield was calculated using the following equation:

$$\text{Hexose yield}\ (\%) = \frac{\text{hexose released}\ (g)}{\text{cellulose content}\ (g)} \times 100$$

2.9. BET

The cellulosic matrix of the WT, *CytoUGE*, and *CpUGE* overexpression lines was extracted through delignification of raw biomass powders using 8 % $NaClO_2$ at 50 °C over a period of two days. The distribution of mesopores and micropores was analyzed using the Micrometrics ASAP 2460 system (USA). Specifically, the Horvath-Kawazoe (HK) method was employed to determine the characteristics of mesopores, while the Barrett–Joyner–Halenda (BJH) approach was utilized for the calculation of micropore distribution.

2.10. Preparation of cellulose nanocrystals

A concentrated sulfuric acid hydrolysis method was used to produce cellulose nanocrystals as previously described (Zhang, Hu, Wang, et al., 2023). First, crude cellulose was prepared from mature stem of WT, *CytoUGE*, and *CpUGE* overexpression lines. The biomass sample was delignified with 8 % $NaClO_2$ at a solid-to- liquid ratio of 1:50 (*w/v*) at 50 °C over a period of two days, and hemicelluloses were removed with 5 % NaOH (w/v) at 50 °C for 1 h (5 times). Then, the samples were washed with deionized water, methanol, and acetone, dehydrated, and dried. Second, the crude cellulose was hydrolyzed to obtain a cellulose nanocrystal colloidal solution. It was hydrolyzed by 64 % sulfuric acid (w/w) at a solid-to-liquid ratio of 1:20 (w/v) at 45 °C for 90 min in a 40 kHz ultra-wave. After stopping hydrolysis with chilled water, the sample was centrifuged to remove excess acid, and the pellets were dialyzed for three days. To prevent aggregation, the colloidal solution was sonicated.

2.11. Characterization of CNCs

For atomic force microscopy (AFM) characterization, the colloidal suspension was diluted to 0.001 % (w/w) using ultrahigh purity water and agitated thoroughly to ensure homogeneity. A 20 μL aliquot of the diluted nanocrystal suspension was drop-cast onto a freshly cleaved mica substrate (approximately 1 cm^2), which was affixed to a 15 mm diameter metal specimen disc using a suitable adhesive. The prepared sample was then mounted onto the AFM sample chuck of a Dimension Icon microscope (Bruker Corporation) for imaging. AFM measurements were performed in PeakForce Tapping Mode (ScanAsyst® in air) using a ScanAsyst-Air-HPI probe (Bruker Corporation) with a nominal spring constant of 0.25 N/m and a resonant frequency of approximately 55 kHz. The cantilever was silicon nitride with a typical tip radius of 2 nm. Imaging was conducted under ambient conditions with a slow scan rate of approximately 1 Hz to ensure high-resolution topography capture and minimize tip-sample interaction forces. For each experiment, three independent biological replicates were analyzed. From the acquired images, a total of 100 individual nanocrystals were randomly selected across different scan areas. Their diameter and length were quantitatively measured using Gwyddion 2.69 software, which provided statistical tools for nanoparticle size distribution analysis.

The nanostructure of the CNCs was further analyzed using transmission electron microscopy (TEM), employing a Talos F200X field-emission gun transmission electron microscope (Thermo Fisher Scientific). TEM imaging was conducted at an accelerating voltage of 200 kV. To mitigate beam-induced damage, a low-dose protocol was implemented during the identification of suitable imaging regions. Additionally, the particle size of the CNCs was measured using a Zetasizer Nano ZS90 instrument (Malvern Instruments Ltd., UK).

2.12. Statistical analysis

All statistical analysis was performed using GraphPad Prism 10.4.0

software. To assess the experimental error, the standard deviation (SD) was calculated as means ± SD. No pairing ordinary ANOVA with Tukey test was used to determine the significant differences in each group. The correlation matrix was computed with a nonparametric Spearman correlation method at two-tailed. Principal component analysis (PCA) with a standardized method was used to classify the WT, *CytoUGE*, and *CpUGE* overexpression line by reducing the dimensions of cell wall parameters.

3. Results

3.1. Genetic engineering of rice plants to enhance UGE from two pathways

Previously, forward genetic studies of classical mutants with deficiencies in growth and stem mechanics have identified two major UDP-glucose epimerases (UGEs) in rice. The two enzymes, which are indispensable for the biosynthesis of UDP-galactose (UDP-Gal), function as crucial components with distinct roles in the cytosol and chloroplast respectively (Liu et al., 2020; Zhang, Wang, et al., 2021). The findings uncovered a distinct spatial segregation of biological functions, which suggests their distinct roles in supplying UDP-Gal for cytosolic and plastidial metabolic pathways. To facilitate clarity in subsequent description, the two genes are henceforth designated as *CytoUGE* (*Os08g0374800*, localized to the cytosol) and *CpUGE* (*Os01g0367100*, specifically within the chloroplast) in this study (Fig. 1A). To dissect how these pathways contribute to plant cell wall polymer biosynthesis and assembly, we generated transgenic rice plants overexpressing *CytoUGE* or *CpUGE*, mimicking increased UDP-Gal availability in the cytosol or chloroplast, respectively (Fig. 1B). For each gene, two genetically stable overexpression lines were selected via qRT-PCR to verify robust transcriptional upregulation (Fig. S1). Notably, regardless of the targeted pathway, elevated UDP-Gal levels consistently led to a reduction in plant height (Fig. 1C), but significantly enhanced tiller number and stem mechanical strength ($P < 0.01$; Fig. 1D, E). These phenotypic data indicate that increasing the UDP-Gal supply via either the cytosolic or chloroplastic pathway promotes tiller development and improves stem mechanics, traits that are closely associated with cell wall integrity. The conserved phenotypic effects of manipulating both pathways suggest a convergent mechanism by which UDP-Gal availability modulates cell wall composition.

3.2. CytoUGE and CpUGE enhanced photosynthesis

One metabolic flux of UDP-Gal is involved in regulating chloroplast development. Considering the close association between chloroplast biogenesis and photosynthetic capacity, we assessed three critical photosynthetic parameters (namely photosynthetic rate, stomatal conductance, and transpiration rate) using a gas exchange and fluorescence detection system. The results showed that all three parameters were markedly elevated in *UGE* overexpression lines (Fig. 2). Notably, *CpUGE* overexpression induced a more pronounced increase in photosynthetic rate than *CytoUGE* overexpression, a difference likely attributed to *CpUGE*'s localization in the chloroplastic pathway (Fig. 2A). Taken together, these data indicate that upregulating the two UDP-Gal biosynthesis pathways can significantly enhance plant photosynthetic capacity. These findings are consistent with previous agronomic trait observations and further suggest a potential link between photosynthetic efficiency and stem mechanical strength (Figs. 1E and 2A).

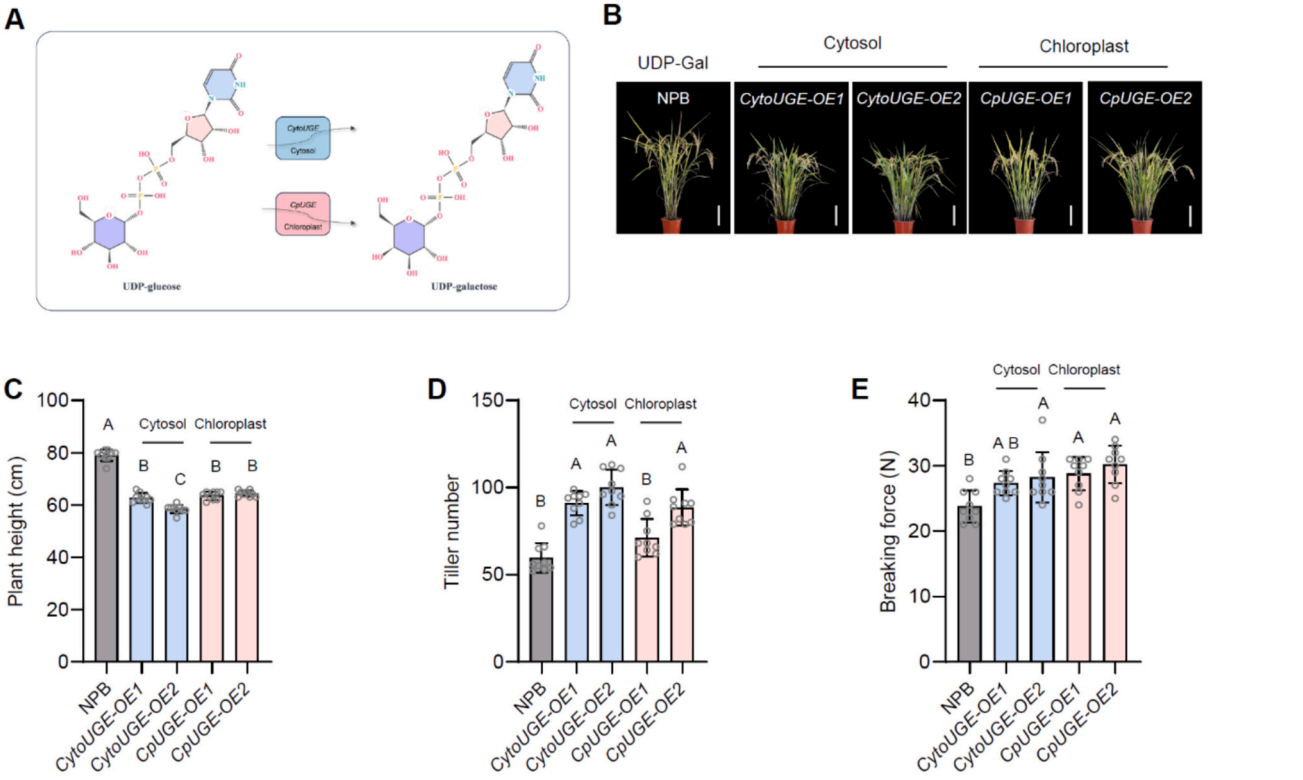

Fig. 1. Genetic engineering of rice to overexpress *UGE* supply via two distinct pathways.
(A) A schematic representation showing the involvement of *CytoUGE* and *CpUGE* in converting UDP-Glucose to UDP-Galactose through two independent pathways, localized in the cytosol and chloroplast, respectively.
(B) Phenotype of genetically engineered rice plants. Scale bar = 15 cm.
(C–E) Quantitative analysis of plant height, tiller number, and stem breaking force for the rice plants shown in (B). Error bars represent ± SD; $n = 9$ biological replicates. Statistical significance was determined using one-way ANOVA with Tukey's multiple-comparisons test ($P < 0.05$).

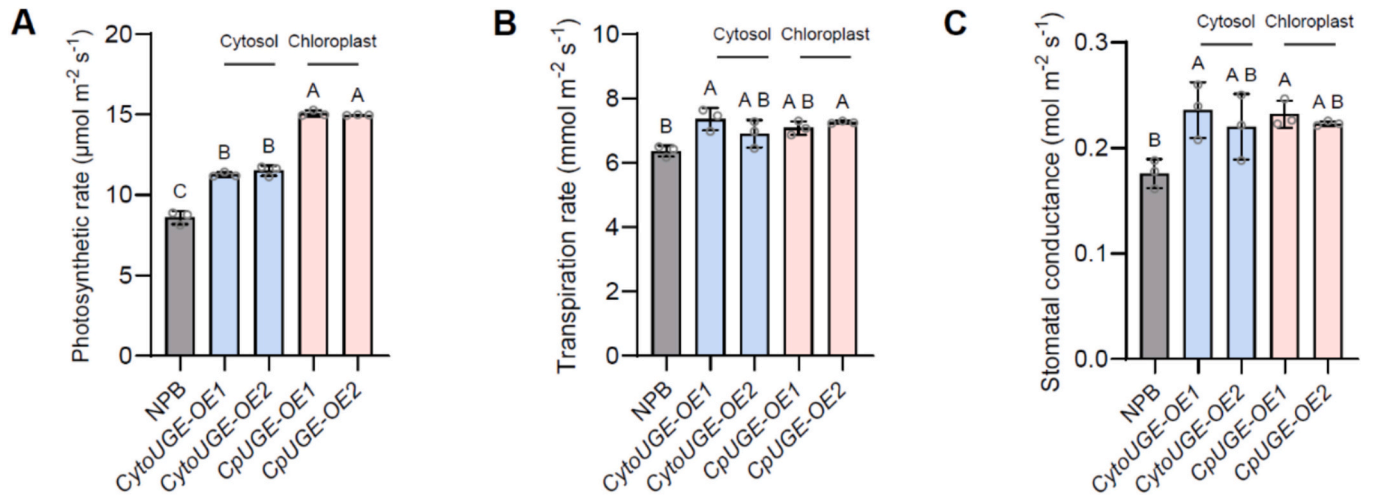

Fig. 2. *CytoUGE* and *CpUGE* influences photosynthesis.
(A–C) Photosynthesis rate, transpiration rate, and stomatal conductance of 60-day-old rice plants. Error bars indicate ± SD; $n = 3$ biological replicates. Statistical significance was assessed using one-way ANOVA with Tukey's multiple-comparisons test ($P < 0.05$).

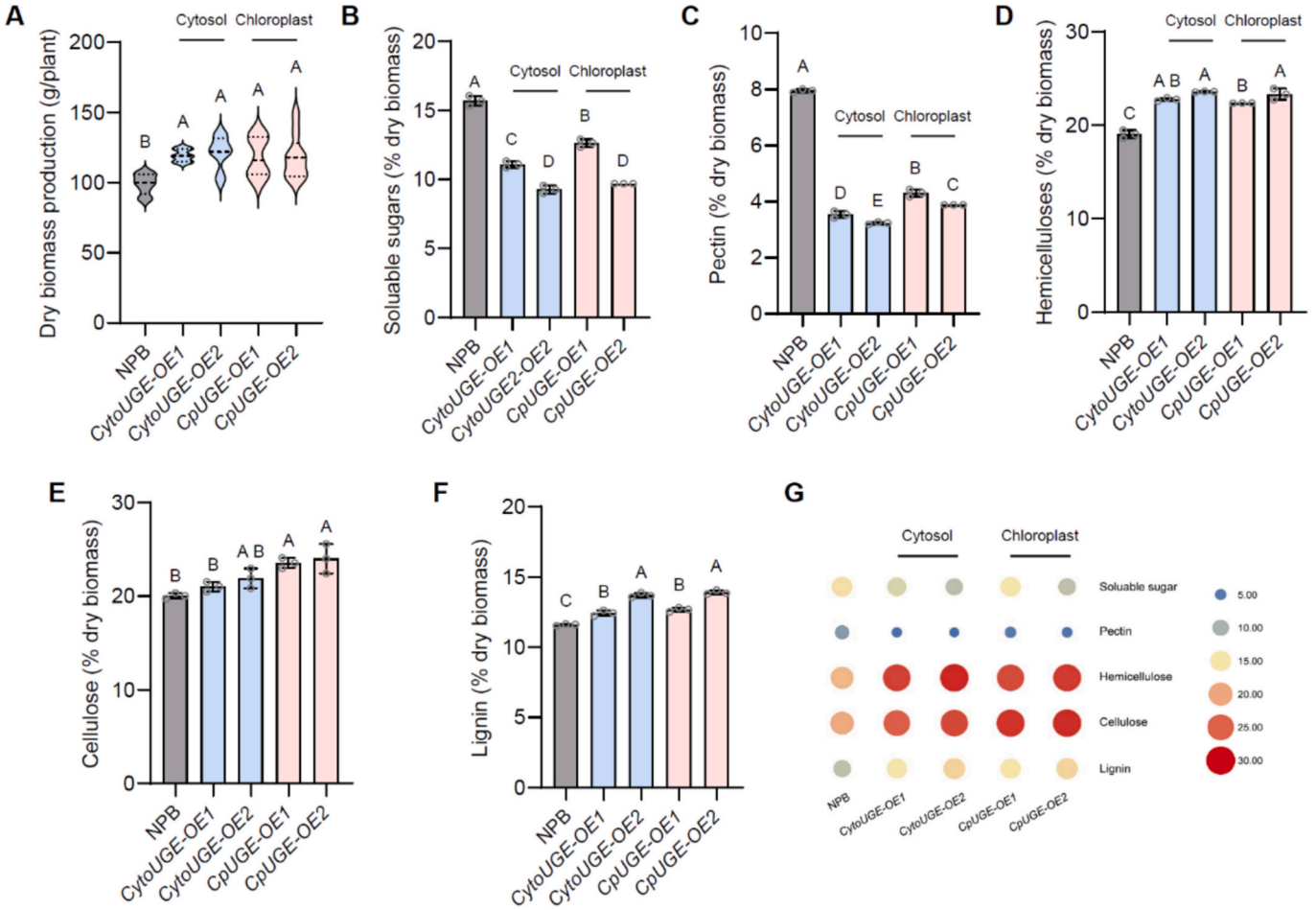

Fig. 3. Impact of *CytoUGE* and *CpUGE* on biomass production and cell wall polymer composition.
(A) Dry biomass production. Error bars represent ± SD; $n = 9$ biological replicates.
(B–E) Sequential extraction and quantification of biomass polysaccharides, including soluble sugars, pectin, hemicellulose, and cellulose content ratios in dry biomass.
(F) Lignin content ratio in dry biomass. Error bars indicate ± SD; $n = 3$ biological replicates. Statistical significance was determined using one-way ANOVA with Tukey's multiple-comparisons test ($P < 0.05$).
(G) Plant cell wall polymer production per plant.

3.3. CytoUGE and CpUGE affects cell wall composition

Photosynthesis is a key determinant of plant biomass accumulation. Given this, we quantified biomass and analyzed cell wall components in mature straw (Fig. 3). The total biomass of *CytoUGE* or *CpUGE* overexpression lines was significantly higher than that of the wild-type (WT) (Fig. 3A), and the trend of biomass variation was highly consistent with the previously observed changes in photosynthetic parameters (Fig. 2). Further analysis of biomass composition revealed consistent relative changes in cell wall components across transgenic lines. Compared to the WT, soluble sugar and pectin contents were significantly reduced (Fig. 3B, C), whereas cellulose, hemicellulose, and lignin contents were markedly increased (Fig. 3D–F). Notably, as cellulose serves as the primary load-bearing component of the cell wall, *CpUGE* overexpression lines exhibited a particularly pronounced increase in cellulose content—an observation that highlights its strong potential to enhance cellulose synthesis and improve plant mechanical properties. To validate the contribution of cellulose to stem mechanics, we performed a supplementary analysis of crystalline cellulose in mature straw (Fig. S2A). The results further confirmed that crystalline cellulose content was significantly elevated in overexpression lines. Moreover, hemicellulose content associated with crystalline cellulose was also significantly increased in all transgenic lines (Fig. S2B). To clarify carbon allocation in biomass, we calculated wall polymer production per plant (Fig. 3G). Data indicated that manipulating UDP-Gal supply was significantly correlated with cellulose and hemicellulose production, suggesting their interactive effects on plant mechanical properties.

3.4. CytoUGE and CpUGE have distinct hemicellulosic interplay

Hemicelluloses act as critical interspatial linkers between cellulose and lignin, rendering their independent chemical extraction nearly impossible. To address this, we performed a detailed analysis of hemicellulosic monosaccharide composition in two distinct fractions: those tightly associated with cellulose and those linked to lignin (Fig. S3A). The 4 M KOH extract, also denoted as the lignin-carbohydrate complex (LCC), represents the lignin-associated fraction, while the non-extracted residue constitutes the cellulose-rich fraction. To quantify total sugar content, we observed increases in both hemicellulose fractions, consistent with wall component analysis (Fig. S3B–C).

First, we conducted neutral monosaccharide composition analysis on the 4 M KOH extract (LCC) derived from crude cell wall samples of transgenic materials (Fig. 4A). The results revealed significant changes in arabinose (Ara), xylose (Xyl), glucose (Glc), and galactose (Gal) contents in *CpUGE* overexpression lines relative to *CytoUGE* overexpression lines (Fig. 4B–E). Xylan, the major hemicellulose, comprises a

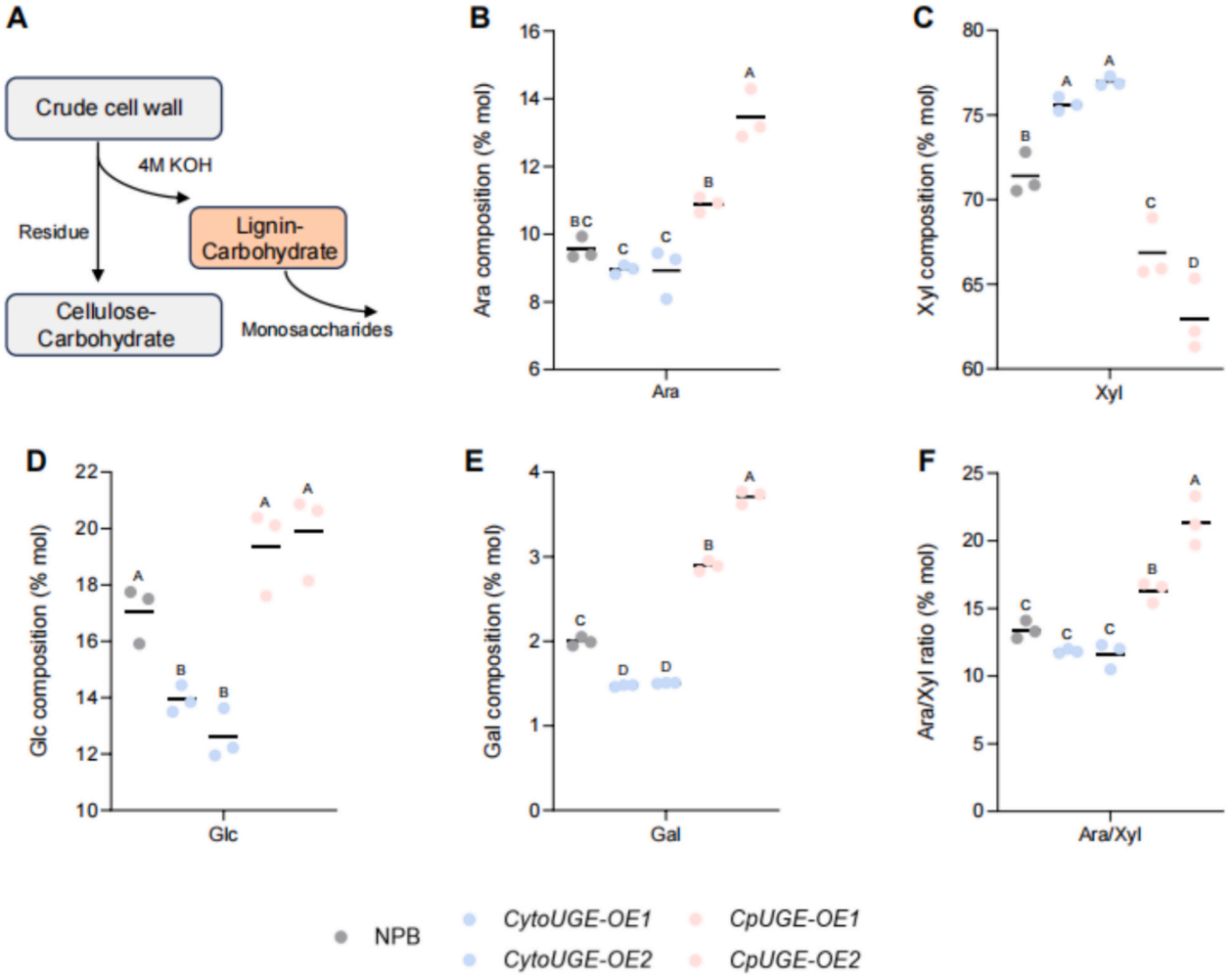

Fig. 4. *CytoUGE* and *CpUGE* modulates monosaccharide composition in lignin-carbohydrate complex (LCC) extracts.
(A) Schematic illustrating the use of 4 M KOH to extract lignin-carbohydrate-rich fractions for neutral monosaccharide determination.
(B–E) Arabinose (Ara), xylose (Xyl), glucose (Glc), and galactose (Gal) contents in the LCC extracts.
(F) Ratio of arabinose to xylose (%) in the LCC extracts. Error bars represent ± SD; $n = 3$ biological replicates. Statistical significance was assessed using one-way ANOVA with Tukey's multiple-comparisons test ($P < 0.05$).

Xyl backbone with Ara side chains. To evaluate xylan branching, we employed the Ara/Xyl ratio. Notably, the xylan branching degree in *CpUGE* overexpression lines was significantly higher, indicating stronger cross-linking with lignin compared to *CytoUGE* overexpression lines (Fig. 4F).

Subsequently, we analyzed the neutral monosaccharide composition of the 4 M KOH non-extracted residue from the crude cell wall of transgenic materials (Fig. 5A). The data showed that manipulating UDP-Gal supply significantly impacted Ara and Xyl levels, whereas Glc and Gal levels remained unchanged (Fig. 5B–E). Under alkaline conditions (4 M KOH), the undissolved fraction following hemicellulose removal corresponds to the cellulose-rich portion, representing hemicellulose tightly cross-linked with cellulose microfibrils. Furthermore, substituted arabinose in confined xylan is thought to bind strongly to cellulose microfibrils (Zhao et al., 2024). By calculating xylan branch substitution, we found that the branching degree (Ara/Xyl ratio) of alkali-insoluble hemicellulose in *CpUGE* overexpression lines was significantly lower (Fig. 5F). This decrease suggests a reduced probability of hemicellulose cross-linking with the non-crystalline regions of cellulose in *CpUGE* overexpression lines, implying less disruption to the cellulose crystalline structure. To validate this, we used the Ara/Glc ratio to assess Ara interference with cellulose (Fig. 5G), and the results were consistent with the Ara/Xyl ratios (Fig. 5F). Collectively, these findings indicate that *CpUGE* overexpression lines exhibit reduced interference from the side chains of confined xylan relative to *CytoUGE* overexpression lines, potentially contributing to their higher crystalline cellulose content.

3.5. *CytoUGE and CpUGE influences cellulosic matrix space*

Based on the characterization of altered major cell wall polymers in *CytoUGE* and *CpUGE* overexpression lines as described above, we further analyzed the wall matrix pore distribution of delignified crude cellulose samples using the Brunauer-Emmett-Teller (BET) method (Fig. 6). Compared with the WT, all *CytoUGE* and *CpUGE* overexpression lines exhibited a remarkably increased nanopore abundance, with distinct pore populations distributed in the 0.5–2 nm (micropore) and 2–50 nm (mesopore) ranges (Fig. 6A–D). BET surface area calculations were consistent with these pore distribution patterns, confirming that the increased nanopore abundance translated to measurable changes in surface area (Fig. S4). Notably, the expanded mesopore (2–50 nm) fraction in *CytoUGE* and *CpUGE* overexpression lines was closely correlated with the space occupied by enhanced lignin content prior to delignification. It aligns with observation that these lines accumulate higher lignin levels. This suggests that lignin deposition in the cell wall matrix may act as a structural scaffold, expanding pore space in the delignified cellulose samples.

3.6. *CytoUGE and CpUGE affects cellulosic feature*

Extending our prior findings that UDP-Gal supply regulates stem

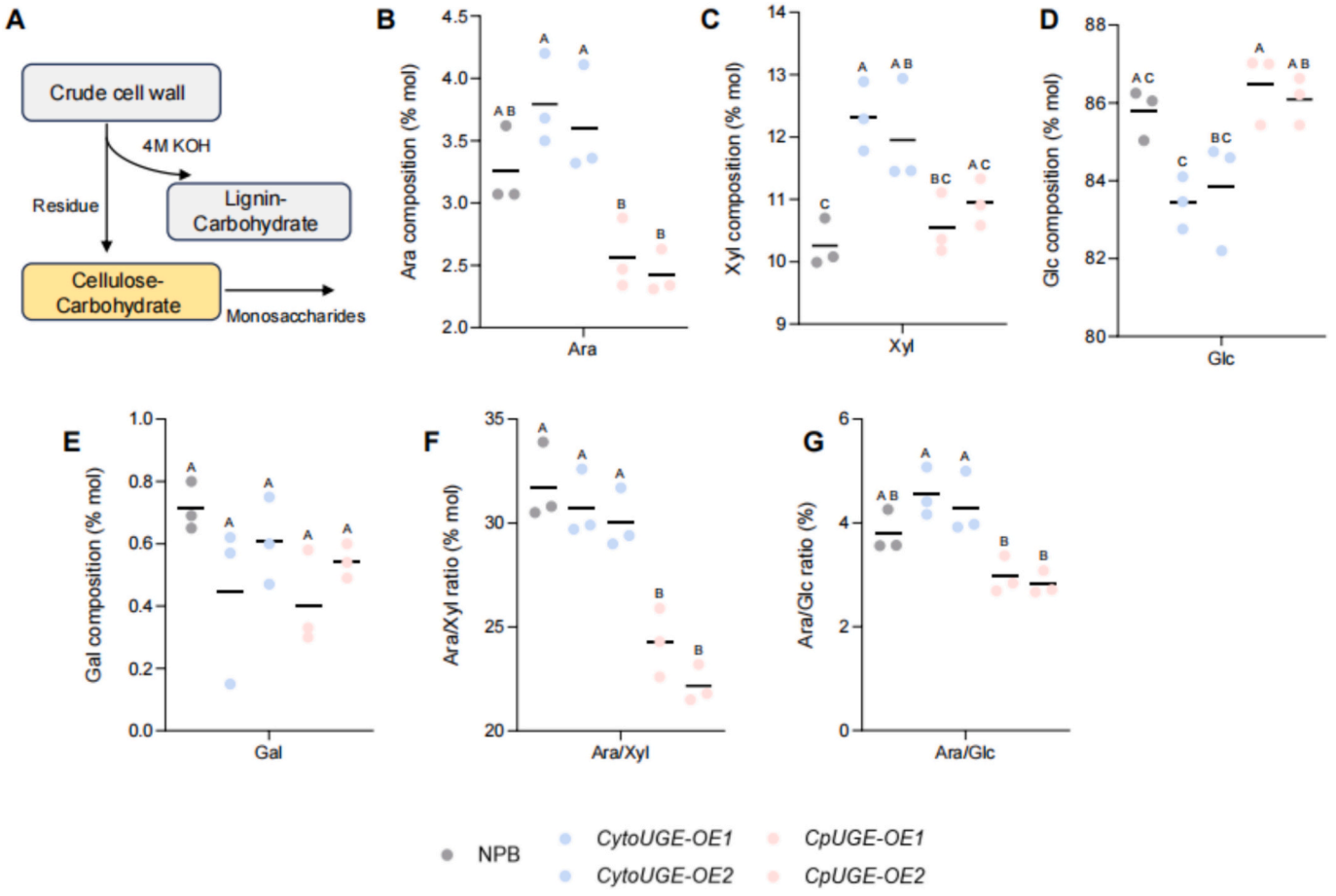

Fig. 5. *CytoUGE* and *CpUGE* alters monosaccharide composition in cellulose-rich residues.
(A) Schematic depicting the extraction of lignin-carbohydrate complexes (LCC) using 4 M KOH, followed by the isolation of cellulose-rich residues for neutral monosaccharide analysis.
(B–E) Arabinose (Ara), xylose (Xyl), glucose (Glc), and galactose (Gal) contents in the cellulose-rich residues.
(F and G) Ratios of arabinose to xylose (%) and arabinose to glucose (%) in the cellulose-rich residues. Error bars indicate ± SD; $n = 3$ biological replicates. Statistical significance was determined using one-way ANOVA with Tukey's multiple-comparisons test ($P < 0.05$).

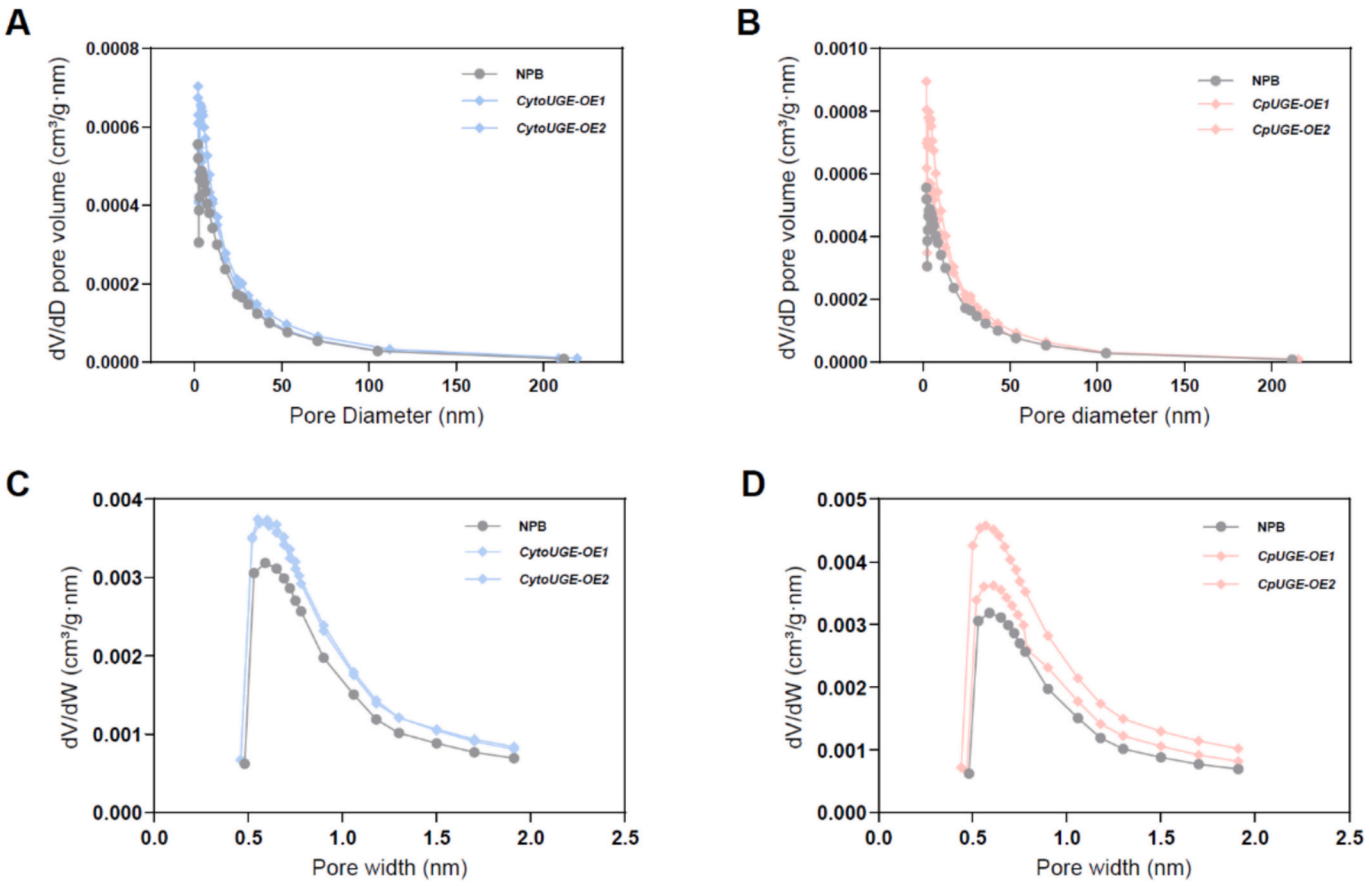

Fig. 6. *CytoUGE* and *CpUGE* influences cellulosic matrix space.
(A and B) BJH adsorption micropore distribution and Horvath-Kawazoe mesopore distribution. (C and D) Horvath-Kawazoe micropore distribution.

mechanical strength through modifications of cellulose structure, we conducted a detailed analysis of cellulose characteristics in mature rice straw. Upon performing 0.5 % NaOH pretreatment followed by enzymatic hydrolysis on these samples, we found that the cellulose degradation efficiency of *CytoUGE* overexpression lines decreased slightly, whereas that of *CpUGE* overexpression lines was significantly lower (Fig. 7A). It confirms that enhancement of the UDP-Gal synthesis pathway markedly improves the anti-degradability of biomass cellulose. Subsequently, we performed X-ray diffraction (XRD) analysis on all raw biomass samples, which revealed diffraction peaks at 2-Theta of 15° (100), 22° (002), and 35° (004) (Fig. 7B, C). These peaks are characteristic of the native type I crystalline structure of cellulose microfibrils, indicating that the samples retained their inherent crystallinity. The cellulose crystallinity index (CrI) was calculated using the Segal method. Results demonstrated that *CpUGE* overexpression lines exhibited the highest CrI values, with the *CpUGE-OE2* transgenic line achieving a notable crystallinity of 49.7 %, the highest among all lines (Fig. 7C). In addition, we tested the viscosity of cellulose chains, and the results

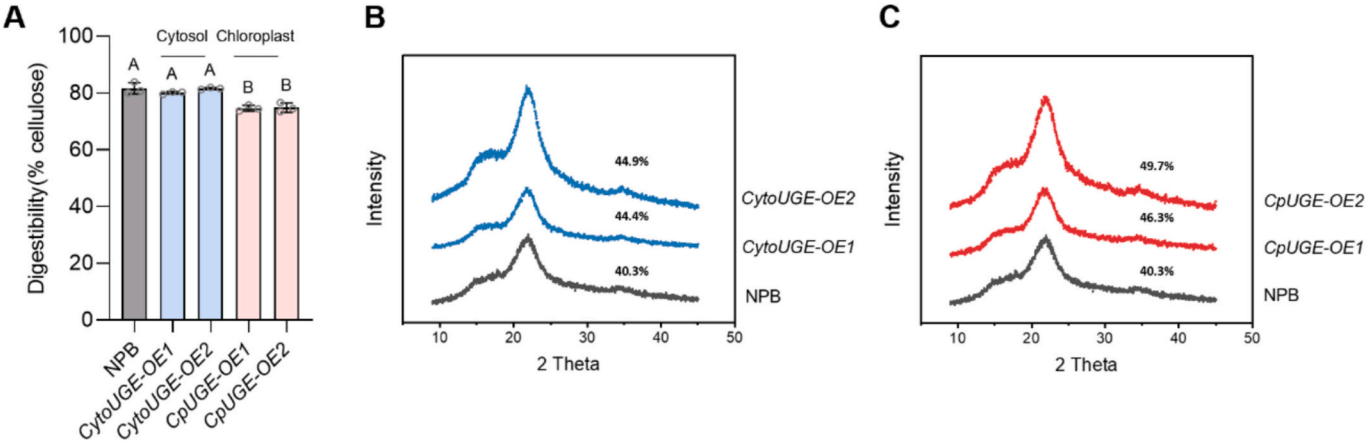

Fig. 7. *CytoUGE* and *CpUGE* affects cellulosic features.
(A) Hexose release following enzymatic hydrolysis after pretreatment with 0.5 % NaOH. Error bars represent ± SD; $n = 3$ biological replicates. Statistical significance was assessed using one-way ANOVA with Tukey's multiple-comparisons test ($P < 0.05$).
(B and C) X-ray diffraction profiles of mature stems. The annotated numbers represent calculated lignocellulosic crystallinity indices (CrI).

confirm that overexpression of *UGE* increases the degree of polymerization of cellulose and its corresponding molecular weight (Fig. S5).The superior cellulose quality of *CpUGE* overexpression lines relative to *CytoUGE* lines aligns with their enhanced stem mechanical strength and reduced interference from xylan side chains—consistent with our earlier observations of minimized disruption to cellulose crystalline structure by xylan side chains in *CpUGE* overexpression lines.

3.7. *CytoUGE and CpUGE with distinct cellulose nanocrystals*

Building on our prior findings that UGEs regulate stem mechanical strength through modifications of cellulose, we elucidated the mechanism underlying the enhanced cellulosic properties observed in all *CytoUGE* and *CpUGE* overexpression lines by conducting a detailed analysis of cellulose nanostructure. As previously demonstrated, cellulose nanocrystal (CNC) dimensions reflect the native cellulose microfibril structure (Zhang, Hu, Peng, et al., 2023). Here, we extracted CNCs from crude cellulose samples via conventional sulfuric acid hydrolysis and quantified their dimensions using atomic force microscopy (AFM; Fig. 8A). Wild-type (WT) CNCs exhibited an average length of 174 nm and diameter of 6.22 nm, whereas *CytoUGE* and *CpUGE* overexpression lines produced significantly larger CNCs with average lengths increased by 30 %–34 % ($P < 0.01$) and modestly enlarged diameters (Fig. 8B, C). The increase in CNC size induced by UGE overexpression was further confirmed by transmission electron microscopy (TEM) and dynamic light scattering (DLS) (Figs. S6, 7). Although the impact of CNC preparation conditions on their resulting size and crystallinity should not be overlooked, it is crucial to emphasize that all CNCs were produced from crude cellulose samples under identical, strictly controlled hydrolysis conditions. Consequently, the observed variations in CNC dimensions and morphology can be ascribed to the inherent differences in the cellulose microfibril structure of the source material, rather than fluctuations in the preparation protocol.

Interestingly, despite all CNCs being subjected to ultrasound treatment prior to AFM analysis, those derived from *CytoUGE* overexpression lines consistently self-assembled into larger aggregates (Fig. 8A). This phenomenon may be attributed to the higher abundance of attached/inserted arabinose side chains in xylan within the cellulose microfibrils of *CytoUGE* overexpression lines (Fig. 5D, F), which could facilitate nanocrystal interactions.

Given that CNCs serve as functional intermediates for high-value bioproduction, the larger CNCs obtained by modulating UDP-Gal supply could be utilized as additives to enhance the mechanical properties of materials. Furthermore, we attempted to produce CNCs from the *cytouge* and *cp-uge* mutants (Fig. S8), which were previously well-characterized as exhibiting growth stunting. Consistent with our expectations, CNCs from these mutants exhibited significant decreases in both length and diameter ($P < 0.05$) (Fig. S9). This size reduction would enhance their high surface-area-to-volume ratios and increase the number of reducing ends available for chemical reactions, making them

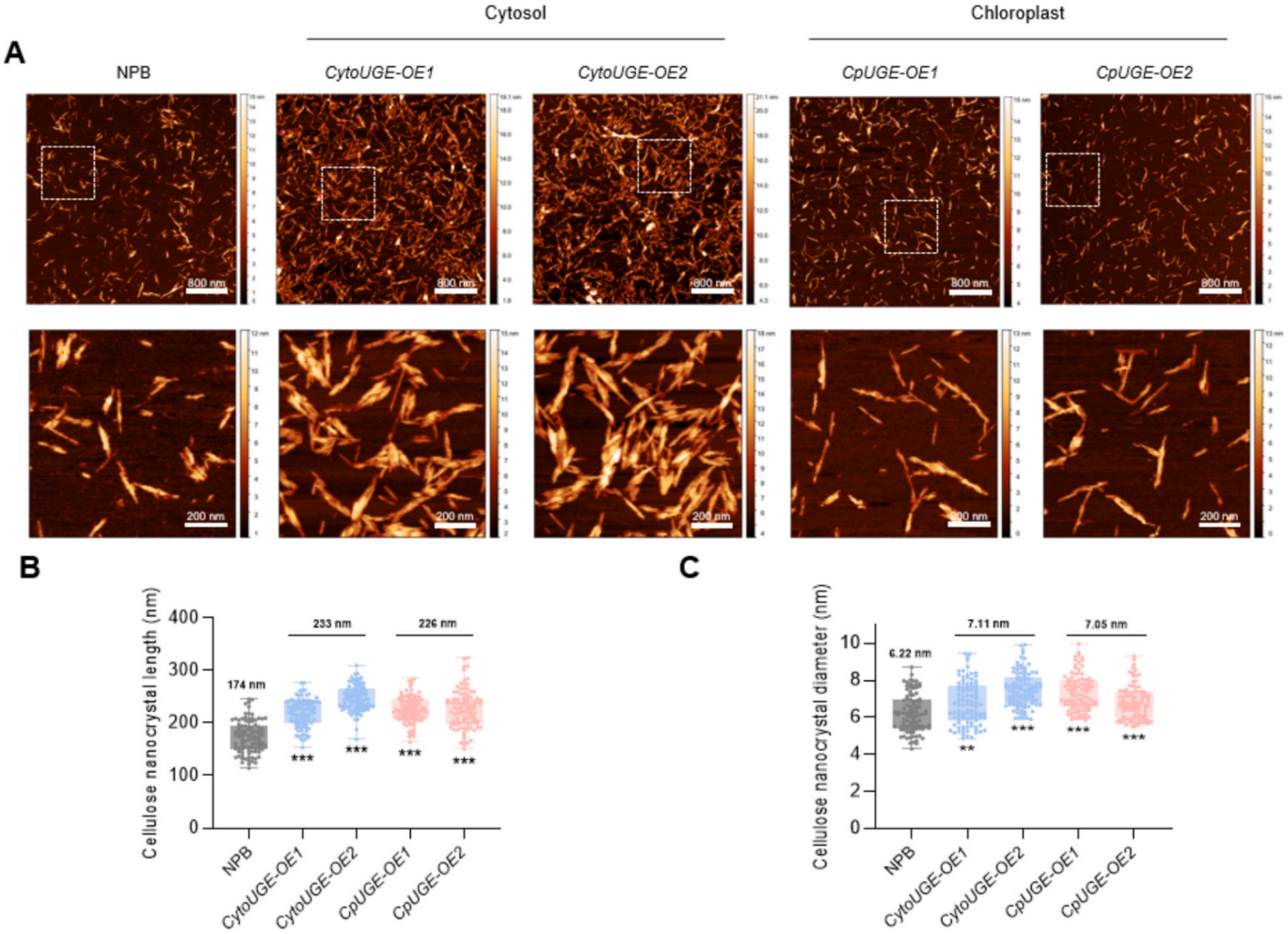

Fig. 8. *CytoUGE* and *CpUGE* influences cellulose nanocrystal dimensions.
(A) Morphological dimensions and measurements of cellulose nanocrystals (B and C). Error bars indicate ± SD; $n = 100$ CNC nanoparticle replicates from 3 biological slice. Statistical significance was determined using one-way ANOVA with Tukey's multiple-comparisons test ($P < 0.05$).

more suitable for applications requiring reactive interfaces. In summary, modulating UDP-Gal supply bidirectionally alters CNC size: overexpression of *CytoUGE/CpUGE* increases CNC dimensions (beneficial for mechanical reinforcement), while loss-of-function mutations (*cyto-uge/cp-uge*) decrease CNC size (advantageous for chemical reactivity) (De France et al., 2021; Tao et al., 2020; Zhao et al., 2022). This versatility enables tailoring of CNC properties to diverse application scenarios.

3.8. Divergence and correlation of CytoUGE and CpUGE plants

To integrate multi-parameter data from cell wall composition, mechanical strength, and photosynthetic measurements, we performed principal component analysis (PCA), which distinctly segregated different plant cell wall samples (Fig. 9A). Notably, cell walls of *CpUGE* overexpression lines were markedly distinct from those of *CytoUGE* overexpression lines. This pattern is consistent with our earlier finding that *CpUGE* plays a more prominent role in modifying cellulose structure than *CytoUGE*. Further, we identified key variables driving this separation: alkali-soluble xylose (Xyl), galactose (Gal), and arabinose (Ara), alongside AIS-Ara/Xyl ratio and the AS-Ara/Xyl ratio (two markers of hemicellulose branching with cellulose and lignin respectively; Fig. 9B). These results indicate that genetic modification of cell wall properties primarily targets hemicellulose structure, which is a component that synergizes with cellulose and lignin to modulate overall cell wall functionality, consistent with our prior hypothesis.

To dissect functional relationships between these variables, we conducted correlation analysis (Fig. 10). Consistent with our prior observations that photosynthesis supports cellulose biosynthesis, photosynthetic rate was negatively correlated with the AIS-Ara/Xyl ratio (indicating reduced hemicellulose branching in insoluble fractions) but positively correlated with the AS-Ara/Xyl ratio (increased branching in soluble fractions) and crystalline cellulose content. Critically, the AIS-Ara/Xyl ratio was negatively associated with cell wall mechanical strength, whereas AS-Ara/Xyl ratio and crystalline cellulose content showed a positive association. These findings directly validate our mechanistic model linking hemicellulose structure to cellulose and lignin assembly and stem rigidity.

Taken together, modulating UDP-Gal supply with UGEs elicits a cascade of effects. Photosynthesis enhanced cellulose biosynthesis, while reduced AIS-Ara/Xyl ratios mitigate hemicellulose-mediated interference with cellulose microfibril. On the other hand, it enhanced AS-Ara/Xyl ratios that generate highly bonded hemicellulose with lignin. Notably, the two Ara/Xyl ratios emerged as key variables connecting UGEs, hemicellulose structure, and mechanical strength. This metric could serve as an indicator for future breeding efforts aimed at optimizing cell wall properties for both crop yield and industrial applications.

3.9. Model of CytoUGE and CpUGE for distinct cell wall assembly

Through the overexpression of *CytoUGE* and *CpUGE* in rice plants, combined with comparative analysis of their functional roles, we propose a model elucidating how these two major types of UGE enhance photosynthesis and stem mechanical strength via distinct cell wall assembly mechanisms (Fig. 11), a finding that diverges significantly from prior studies focused solely on UGE expression levels (Li et al., 2011; Liu et al., 2020; Zhang, Wang, et al., 2021). Our study uniquely demonstrates that both CytoUGE and CpUGE boost photosynthetic efficiency and stem mechanical integrity by driving accumulation of major cell wall polymers. Notably, when comparing their functions, CpUGE exerts a more profound impact on both photosynthesis and mechanical performance. Contrary to earlier work emphasizing cellulose content as the primary strength determinant (Hu et al., 2018; Li et al., 2017), we reveal that the superior stem strength conferred by CpUGE arises not only from

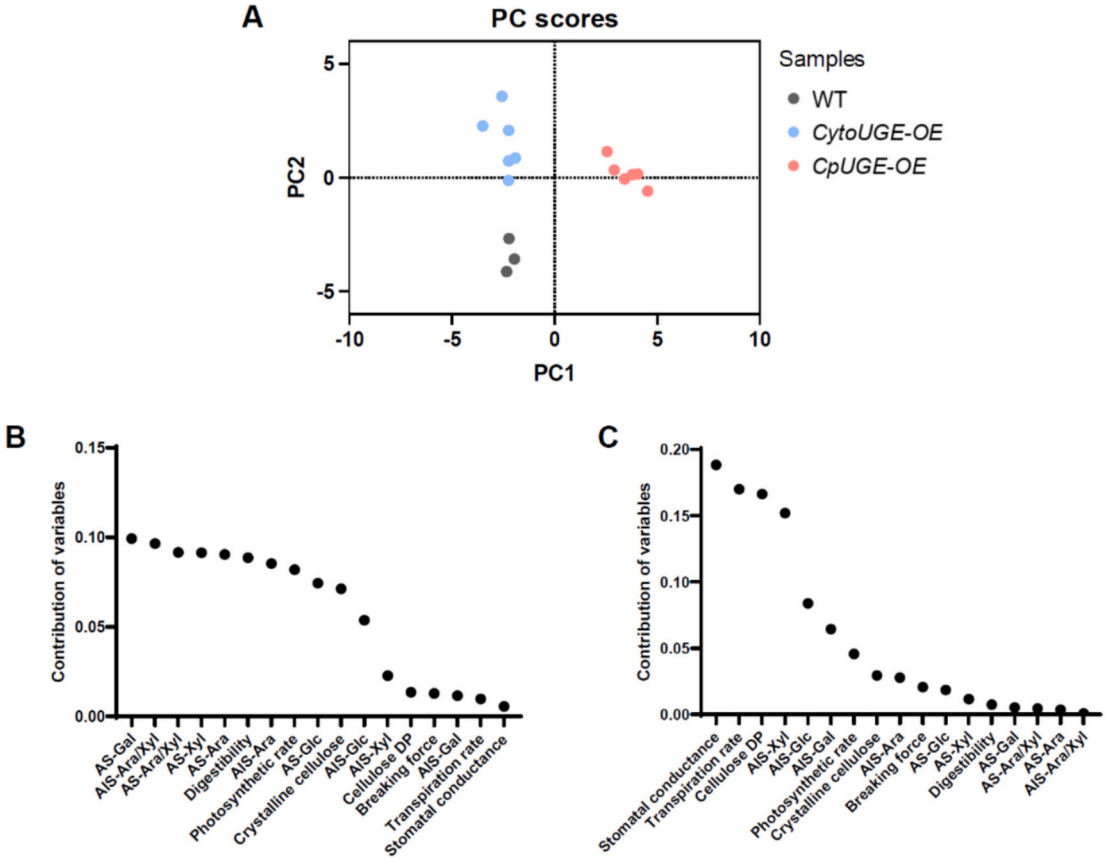

Fig. 9. Principal component analysis of all cell wall compositions and associated factors.

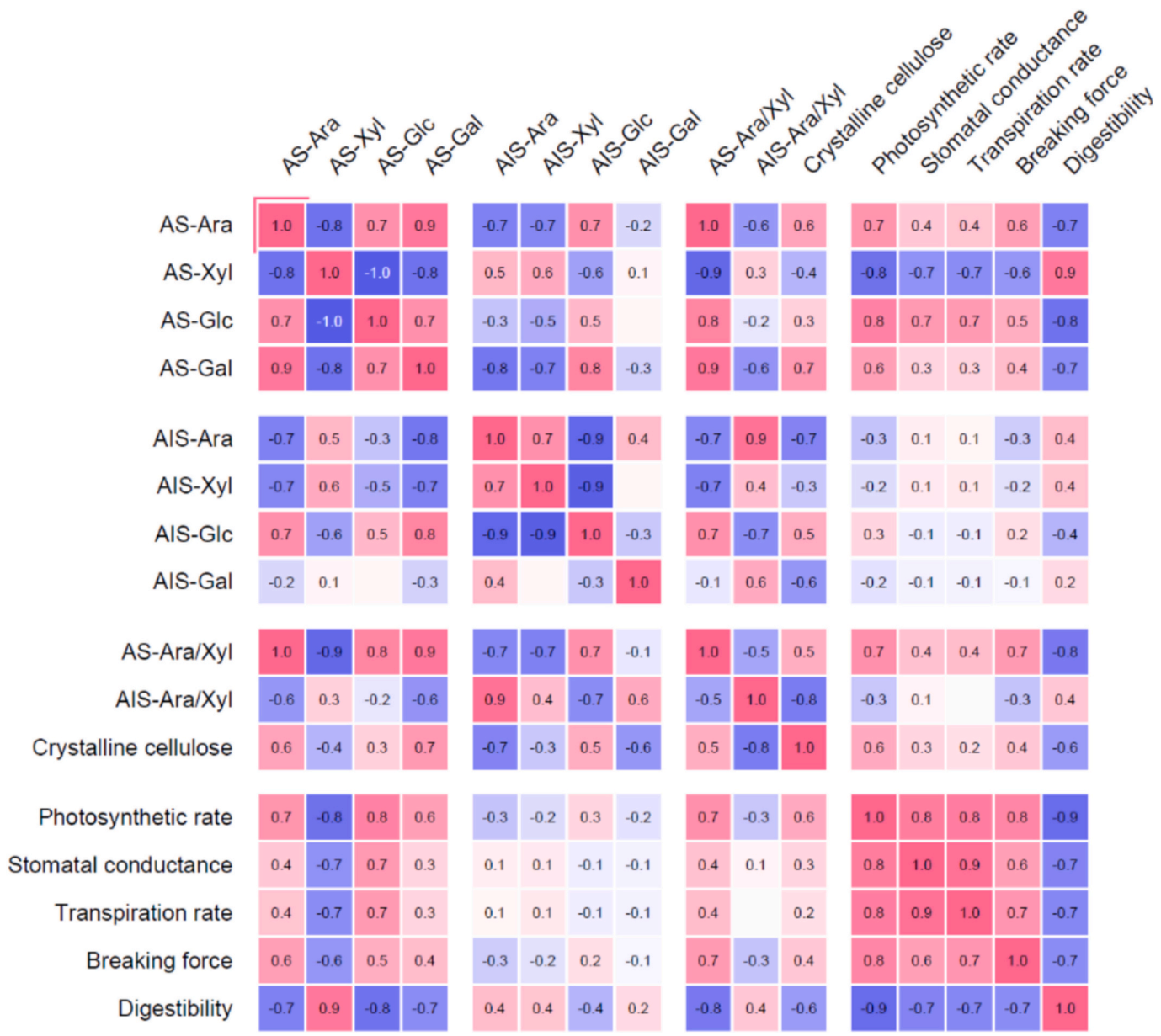

Fig. 10. Correlation analysis among all cell wall compositions and factors Two-tailed Spearman's correlation analysis was performed.

its higher cellulose content and improved cellulose quality but also from its unique cell wall architecture. Relative to CytoUGE and previous models, which overlooked xylan-lignin interactions, we show that the arabinose side chains of xylan in CpUGE exhibit a closer association with lignin and interfere less with cellulose microfibril alignment. This distinctive cell wall architecture is further manifested in the striking bidirectional modifications of CNCs derived from the two distinct UGEs. These findings also serve as a complement to our earlier work, which demonstrated a unidirectional modulation of CNCs through the engineering of cellulose synthesis subunits (Zhang, Hu, Wang, et al., 2023). Collectively, these insights establish a novel dual-regulatory paradigm for UGE-mediated cell wall assembly, providing critical targets for engineering high-strength, photosynthetic-efficient crops.

4. Conclusions

Our findings confirm the initial hypothesis that cytosolic and chloroplastic UGEs exert distinct, compartment-specific effects on cell wall assembly in rice. We demonstrate that both CytoUGE and CpUGE overexpression lines enhanced photosynthesis and increased the abundance of cellulose, hemicellulose, and lignin, leading to improved stem mechanical strength—a convergent outcome validating their shared role in biomass reinforcement. Critically, however, CpUGE overexpression had a significantly more pronounced effect on cellulose accumulation and crystallinity. This superior performance is mechanistically linked to CpUGE's chloroplastic localization, which fosters a more ordered cell wall architecture: tighter xylan-lignin interactions in the soluble fraction and reduced arabinose substitution in alkali-insoluble xylan, thereby minimizing interference with cellulose microfibril alignment. In contrast, while CytoUGE also strengthens the cell wall, it does so with greater xylan branching in the cellulose-rich matrix, leading to CNCs that are prone to self-aggregation. This divergence underscores the spatial regulation of nucleotide sugar metabolism—the chloroplastic pathway CpUGE is uniquely positioned to more effectively channel photosynthetic output into high-quality cellulose assembly. Furthermore, our work confirms the bidirectional tunability of CNC dimensions for potential bioproduction uses through UGE modulation. In summary, this study not only validates our initial hypothesis but also establishes a

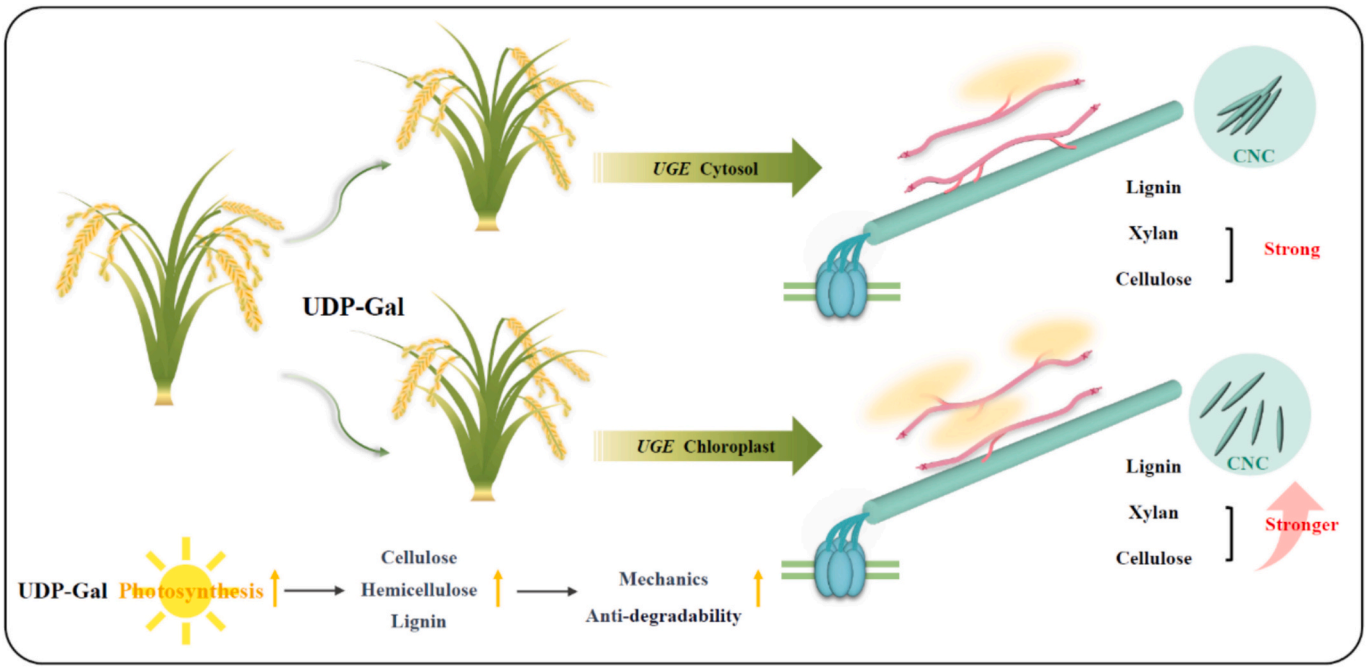

Fig. 11. Proposed model: *CytoUGE* and *CpUGE* enhance plant photosynthesis and plant mechanics through distinct assembly of cell wall polymers in rice.

strategic framework for precision engineering of lignocellulosic biomass. By exploiting the spatial separation of metabolic pathways, we can tailor rice varieties for either enhanced agronomic resilience or optimized production of size-tunable cellulose nanomaterials for industrial applications.

CRediT authorship contribution statement

Yumeng Sun: Visualization, Methodology, Investigation, Formal analysis. **Muzi Li:** Visualization, Methodology, Investigation, Formal analysis. **Meiyun Yang:** Methodology, Investigation. **Wennian Xia:** Methodology, Investigation. **Sha Wang:** Methodology, Investigation. **Zhongyi Wang:** Methodology, Investigation. **Yanting Wang:** Writing – review & editing, Supervision. **Liangcai Peng:** Writing – review & editing, Supervision. **Huizhen Hu:** Writing – review & editing, Supervision, Funding acquisition, Conceptualization. **Ran Zhang:** Writing – review & editing, Writing – original draft, Supervision, Investigation, Funding acquisition, Conceptualization.

Declaration of competing interest

The authors declare that they have no known competing financial interests or personal relationships that could have appeared to influence the work reported in this paper.

Acknowledgments

The project was supported by the National Natural Science Foundation of China (grant No. 32460067 and 32100214), Yunnan Fundamental Research Projects (grant No. 202401BF070001-001 and 202501AW070018), Yunnan Provincial High-level Talents Introduction of Young Talents Special Competitive Training Support Funds (grant No. YNQR-QNRC-2018-122), Scientific Research Fund of Yunnan Educational Commission and the Graduate Scientific Research Innovation Foundation of Yunnan University (grant No. KC-252513592).

Appendix A. Supplementary data

Supplementary data to this article can be found online at https://doi.org/10.1016/j.carbpol.2025.124803.

Data availability

All data supporting the findings of the present study are available in the article and Supplementary.

References

Barber, C., Rösti, J., Rawat, A., Findlay, K., Roberts, K., & Seifert, G. J. (2006). Distinct properties of the five UDP-D-glucose/UDP-D-galactose 4-epimerase isoforms of *Arabidopsis thaliana*. *The Journal of Biological Chemistry, 281*(25), 17276–17285.

Bar-Peled, M., & O'Neill, M. A. (2011). Plant nucleotide sugar formation, interconversion, and salvage by sugar recycling. *Annual Review of Plant Biology, 62*, 127–155.

Coen, E., & Cosgrove, D. J. (2023). The mechanics of plant morphogenesis. *Science, 379*(6631), Article eade8055.

Cosgrove, D. J. (2018). Nanoscale structure, mechanics and growth of epidermal cell walls. *Current Opinion in Plant Biology, 46*, 77–86.

Cosgrove, D. J. (2022). Building an extensible cell wall. *Plant Physiology, 189*(3), 1246–1277.

De France, K., Zeng, Z., Wu, T., & Nyström, G. (2021). Functional materials from nanocellulose: Utilizing structure-property relationships in bottom-up fabrication. *Advanced Materials, 33*(28), Article e2000657.

Herburger, K., Franková, L., Pičmanová, M., Loh, J. W., Valenzuela-Ortega, M., Meulewaeter, F., … Fry, S. C. (2020). Hetero-trans-β-glucanase produces cellulose-xyloglucan covalent bonds in the cell walls of structural plant tissues and is stimulated by expansin. *Molecular Plant, 13*(7), 1047–1062.

Hu, H., Zhang, R., Feng, S., Wang, Y., Wang, Y., Fan, C., … Peng, L. (2018). Three AtCesA6-like members enhance biomass production by distinctively promoting cell growth in *Arabidopsis*. *Plant Biotechnology Journal, 16*(5), 976–988.

Ishida, K., & Noutoshi, Y. (2022). The function of the plant cell wall in plant-microbe interactions. *Plant Physiology and Biochemistry, 192*, 273–284.

Li, C., Wang, Y., Liu, L., Hu, Y., Zhang, F., Mergen, S., … Chu, C. (2011). A rice plastidial nucleotide sugar epimerase is involved in galactolipid biosynthesis and improves photosynthetic efficiency. *PLoS Genetics, 7*(7), Article e1002196.

Li, F., Xie, G., Huang, J., Zhang, R., Li, Y., Zhang, M., … Peng, L. (2017). *OsCESA9* conserved-site mutation leads to largely enhanced plant lodging resistance and biomass enzymatic saccharification by reducing cellulose DP and crystallinity in rice. *Plant Biotechnology Journal, 15*(9), 1093–1104.

Li, W., Lin, Y. J., Chen, Y. L., Zhou, C., Li, S., De Ridder, N., … Chiang, V. L. (2024). Woody plant cell walls: Fundamentals and utilization. *Molecular Plant, 17*(1), 112–140.

Liu, S., Tang, Y., Ruan, N., Dang, Z., Huang, Y., Miao, W., Xu, Z., & Li, F. (2020). The rice BZ1 locus is required for glycosylation of arabinogalactan proteins and galactolipid and plays a role in both mechanical strength and leaf color. *Rice, 13*(1), 41.

Molina, A., Jordá, L., Torres, M.Á., Martín-Dacal, M., Berlanga, D. J., Fernández-Calvo, P., … Martín-Santamaría, S. (2024). Plant cell wall-mediated disease

resistance: Current understanding and future perspectives. *Molecular Plant, 17*(5), 699–724.
Ray, U., Zhu, S., Pang, Z., & Li, T. (2021). Mechanics design in cellulose-enabled high-performance functional materials. *Advanced Materials, 33*(28), Article e2002504.
Rösti, J., Barton, C. J., Albrecht, S., Dupree, P., Pauly, M., Findlay, K., … Seifert, G. J. (2007). UDP-glucose 4-epimerase isoforms UGE2 and UGE4 cooperate in providing UDP-galactose for cell wall biosynthesis and growth of *Arabidopsis thaliana*. *The Plant Cell, 19*(5), 1565–1579.
Seifert, G. J. (2004). Nucleotide sugar interconversions and cell wall biosynthesis: How to bring the inside to the outside. *Current Opinion in Plant Biology, 7*(3), 277–284.
Seifert, G. J., Barber, C., Wells, B., & Roberts, K. (2004). Growth regulators and the control of nucleotide sugar flux. *The Plant Cell, 16*(3), 723–730.
Tao, H., Lavoine, N., Jiang, F., Tang, J., & Lin, N. (2020). Reducing end modification on cellulose nanocrystals: Strategy, characterization, applications and challenges. *Nanoscale Horizons, 5*(4), 607–627.
Updegraff, D. M. (1969). Semimicro determination of cellulose in biological materials. *Analytical Biochemistry, 32*(3), 420–424.
Verbančič, J., Lunn, J. E., Stitt, M., & Persson, S. (2018). Carbon supply and the regulation of cell wall synthesis. *Molecular Plant, 11*(1), 75–94.
Wan, J., He, M., Hou, Q., Zou, L., Yang, Y., Wei, Y., & Chen, X. (2021). Cell wall associated immunity in plants. *Stress Biology, 1*(1), 3.
Wang, X., Du, T., Huang, J., Peng, S., & Xiong, D. (2018). Leaf hydraulic vulnerability triggers the decline in stomatal and mesophyll conductance during drought in rice. *Journal of Experimental Botany, 69*(16), 4033–4045.
Wang, X., Han, J., Pang, S., Li, J., Zhao, J., Qin, C., Yao, S., Liu, Y., & Liang, C. (2022). Structural enrichment and identification of lignin-carbohydrate complex in alkaline stabilized system. *Carbohydrate Polymers, 296*, Article 119873.
Wang, Y., Fan, C., Hu, H., Li, Y., Sun, D., Wang, Y., & Peng, L. (2016). Genetic modification of plant cell walls to enhance biomass yield and biofuel production in bioenergy crops. *Biotechnology Advances, 34*(5), 997–1017.
Xie, K., Minkenberg, B., & Yang, Y. (2015). Boosting CRISPR/Cas9 multiplex editing capability with the endogenous tRNA-processing system. *Proceedings of the National Academy of Sciences of the United States of America, 112*(11), 3570–3575.
Xu, N., Zhang, W., Ren, S., Liu, F., Zhao, C., Liao, H., Xu, Z., Huang, J., Li, Q., Tu, Y., Yu, B., Wang, Y., Jiang, J., Qin, J., & Peng, L. (2012). Hemicelluloses negatively affect lignocellulose crystallinity for high biomass digestibility under NaOH and H_2SO_4 pretreatments in *Miscanthus*. *Biotechnology for Biofuels, 5*(1), 58.
Yu, H., Hu, M., Hu, Z., Liu, F., Yu, H., Yang, Q., Gao, H., Xu, C., Wang, M., Zhang, G., Wang, Y., Xia, T., Peng, L., & Wang, Y. (2022). Insights into pectin dominated enhancements for elimination of toxic Cd and dye coupled with ethanol production in desirable lignocelluloses. *Carbohydrate Polymers, 286*, Article 119298.
Yu, H., Zhang, G., Liu, J., Liu, P., Peng, H., Teng, Z., … Peng, L. (2025). A functional cascading of lignin modification via repression of caffeic acid O-methyltransferase for bioproduction and anti-oxidation in rice. *Journal of Advanced Research, 78*, 1–9.
Zhang, B., Gao, Y., Zhang, L., & Zhou, Y. (2021). The plant cell wall: Biosynthesis, construction, and functions. *Journal of Integrative Plant Biology, 63*(1), 251–272.
Zhang, R., Gao, H., Wang, Y., He, B., Lu, J., Zhu, W., Peng, L., & Wang, Y. (2023). Challenges and perspectives of green-like lignocellulose pretreatments selectable for low-cost biofuels and high-value bioproduction. *Bioresource Technology, 369*, Article 128315.
Zhang, R., Hu, H., Wang, Y., Hu, Z., Ren, S., Li, J., He, B., Wang, Y., Xia, T., Chen, P., Xie, G., & Peng, L. (2020). A novel rice *fragile culm 24* mutant encodes a UDP-glucose epimerase that affects cell wall properties and photosynthesis. *Journal of Experimental Botany, 71*(10), 2956–2969.
Zhang, R., Hu, Z., Peng, H., Liu, P., Wang, Y., Li, J., Lu, J., Wang, Y., Xia, T., & Peng, L. (2023). High density cellulose nanofibril assembly leads to upgraded enzymatic and chemical catalysis of fermentable sugars, cellulose nanocrystals and cellulase production by precisely engineering cellulose synthase complexes. *Green Chemistry, 25*(3), 1096–1106.
Zhang, R., Hu, Z., Wang, Y., Hu, H., Li, F., Li, M., Ragauskas, A., Xia, T., Han, H., Tang, J., Yu, H., Xu, B., & Peng, L. (2023). Single-molecular insights into the breakpoint of cellulose nanofibers assembly during saccharification. *Nature Communications, 14*(1), 1100.
Zhang, Y., Wang, Y., Wang, C., Rautengarten, C., Duan, E., Zhu, J., … Wan, J. (2021). *BRITTLE PLANT1* is required for normal cell wall composition and mechanical strength in rice. *Journal of Integrative Plant Biology, 63*(5), 865–877.
Zhao, H., Wang, S., Yang, R., Yang, D., Zhao, Y., Kuang, J., Chen, L., Zhang, R., & Hu, H. (2024). Side chain of confined xylan affects cellulose integrity leading to bending stem with reduced mechanical strength in ornamental plants. *Carbohydrate Polymers, 329*, Article 121787.
Zhao, X., Wang, Q., Zhu, G., Ma, J., & Lin, N. (2022). Size effect of cellulose nanocrystals in cellular internalization and exosome-packaging exocytosis. *Carbohydrate Polymers, 298*, Article 120131.